JOURNAL OF CATALYSIS 134, 594–607 (1992)

Preparation of Ternary Cu/Co/Al Catalysts by the Amorphous Citrate Process

II. The Effect of the Decomposition–Calcination Atmosphere

J. I. DI COSIMO[1], A. J. MARCHI, AND C. R. APESTEGUIA[2]

Instituto de Investigaciones en Catálisis y Petroquímica-INCAPE-Santiago del Estero 2654, (3000) Santa Fe, Argentina

Received September 17, 1991

The effect of the decomposition–calcination procedure of Cu/Co/Al citrate precursors on the characteristics of the resulting mixed oxides and on the catalytic activity and selectivity for synthesis gas conversion to methanol and higher alcohols was studied. Cu/Co/Al amorphous precursors were prepared by means of the citric complexing method. Four different decomposition–calcination procedures were employed: I, air–air 500°C; II, N_2–N_2 500°C; III, N_2 500°C–air 500°C, and IV, N_2 280°C–air 500°C. The physicochemical properties of the mixed oxides (major surface species, porous structure, binary phases) were influenced by the decomposition–calcination procedure employed. The mixed oxides obtained through procedure II had low surface areas (8 $m^2\ g^{-1}$), large particles of Cu and Co in metallic state, and high amounts of residual carbon. As a consequence, the catalytic activity was low and the selectivity to hydrocarbons was enhanced up to 70 wt%. Procedure III eliminated the residual carbon and regenerated metal oxides phases. However, the surface area was still low (14 $m^2\ g^{-1}$) and a Cu-rich layer was formed at the sample surface, thereby causing an inhomogeneous distribution of the metal ions. These catalysts exhibited poor higher alcohol selectivities. The mixed oxides obtained through procedures I and IV exhibited similar physicochemical properties and catalytic activities. XRD and TPR characterization identified the formation of CuO and Co_3O_4 oxides and $Co(Cu)Al_2O_4$ aluminates. Surface species were mostly CuO and Co_3O_4. The distribution of the metals was uniform and the surface area values were relatively high (60–65 $m^2\ g^{-1}$). These catalysts exhibited higher catalytic activity and were selective for the formation of alcohols, producing 52–54 wt% of total alcohols and 23–25 wt% of ethanol and higher alcohols. The catalytic results suggest that the homogeneous distribution of the metallic elements is crucial to higher alcohol synthesis.

INTRODUCTION

Ternary and quaternary mixed oxide catalysts, such as Cu/Co/(Zn)/Al(Cr) modified by alkali salts, readily catalyze the conversion of synthesis gas ($CO/CO_2/H_2$) to methanol and higher alcohols under low-pressure conditions (*1–4*). Studies detailing both the catalytic system and the optimization process conditions were initially reported by industrial research groups, especially the Institut Français du Pétrole (*5–7*). Recently, a number of fundamental studies concerning the influence of preparation procedures on the catalytic performance have been published (*8–12*). In all cases, it was stated that the activity and selectivity of the catalysts were dependent on preparation parameters, in particular thermal activation, thereby suggesting that catalyst preparation is a critical factor. This fact is due not only to the characteristics of the catalytic system and the need of obtaining reproducible final cata-

[1] Present address: Department of Chemistry, Lehigh University, Bethlehem, PA 18015.

[2] Present address: EXXON Research and Engineering Co., Corporate Research, Route 22 East, Annandale, NJ 08801.

0021-9517/92 $3.00

lysts, but also to the nature of the active sites involved in the chain growth mechanisms responsible for the synthesis of higher alcohols (*13–15*).

A previous paper (*16*) presented the results of a detailed study of the preparation of Cu/Co/Al precursors by the amorphous citrate process. The complexation method (*17–19*) normally allows the preparation of amorphous and homogeneous precursors. In addition, in the case of quaternary catalysts, this method has the advantage that the alkaline promoter can be included from the start. However, the exothermic air decomposition of these glassy precursors is difficult to control when the solid contains a metal catalytically active in oxidation reactions (*20*).

Reasoning that the instability of the precursors was most likely related to nitration of citric acid, Sheffer and King (*21*) investigated the possibility of using metal acetate salts instead of metal nitrates. They found that the limited water solubility of cupric acetate yielded inhomogeneous precursors, which lead to catalysts having poor oxygenate selectivity. On the other hand, Zhang *et al.* (*22*) showed that for single-phase perovskite formation, a citrate decomposition process requires a calcination temperature 200–300°C lower than the acetate process. The lower calcination temperature results in the formation of oxides with higher BET surface areas.

Another technique for controlling the exothermic precursor decomposition would be to reduce the oxygen concentration in the nitrogen–oxygen mixture used as decomposition atmosphere. We have previously described the influence of the decomposition atmosphere on the characteristics of the main exothermic transformations occurring during the overall decomposition of hydroxycitrate precursors (*16*). We studied the decomposition in air and, as a limiting case, the decomposition in N_2. Two additional decomposition procedures consisting of consecutive N_2–air treatments were also investigated. We concluded that "a two-step decomposition procedure using first nitrogen up to 280°C and after that an oxygen-containing atmosphere to oxidize the organic part at relatively low temperature will be more appropriate to avoid the danger of an uncontrolled exothermic decomposition (direct decomposition in air) or the problems derived from a contamination with residual carbon (decomposition in N_2 up to 500°C)" (*16*). However, this conclusion referred only to the most suitable procedure regarding the control of the highly exothermic decomposition. In the present paper we have extended the studies to include the influence of these different decomposition treatments on the characteristics of the resulting mixed oxides and on the catalytic activity and selectivity toward methanol and higher alcohols from synthesis gas. The calcination step was also included, and thus the mixed oxides were produced using different decomposition–calcination procedures.

EXPERIMENTAL

Preparation of Mixed Oxides

Ternary Cu/Co/Al precursor A was prepared by the complexation method described in (*16*). Citric acid was added to a concentrated aqueous solution that contained all the required ions as metal nitrates. An acid/metal ratio of 1 g-eq of acid/total g-eq of metals was used. The solution was initially held at boiling temperature for 20–30 min and was then evaporated under vacuum in a revolving flask at 75°C until a viscous liquid was obtained. Finally, dehydration was completed by drying the sample in a vacuum oven at 80°C for 13 h. Chemical analysis showed that the atomic ratios of the metallic elements in hydroxycitrate precursor A were Cu/Co = 0.96 and (Cu + Co)/Al = 1.02. The mixed oxides were obtained from precursor A by using four different decomposition–calcination procedures. Details of these procedures are given in Table 1. The experiments were performed at atmospheric pressure in a flow system provided with a fixed-bed reactor. In the decomposition step, the temperature was raised 1°C

min^{-1} from 25°C to T_M, the final decomposition temperature. After that, samples were calcined by heating at 1°C min^{-1} from 25 to 500°C and holding at this temperature for 8 h. The flow rate of nitrogen and air was 30 ml min^{-1}.

Characterization of Mixed Oxides

Powder X-ray diffraction patterns (XRD) were collected on a Rich–Seifert diffractometer using a nickel filtered Cu$K\alpha$ radiation. Crystallite dimensions were evaluated using the Scherrer equation.

The temperature-programmed reduction (TPR) experiments were carried out with a gaseous mixture containing 5% H_2 in argon. The flow rate of the reducing gas was 20 cm^3 min^{-1}. Samples were heated with a linear temperature programmer-controlled electric furnace at 5°C min^{-1} within the temperature range 20–900°C. Since water is formed during sample reduction, the gas exiting from the reactor was passed through a cold trap before entering the thermal conductivity cell. The TCD was a flow-through type, microvolume, hot wire Gow Mac cell. Hydrogen uptakes were estimated by integration of the TPR signal. CuO samples were used as reference for quantitative analysis. In order to identify the H_2 consumption peaks, mono- and bimetallic oxides of Cu, Co, and Al were prepared and characterized by TPR (*9, 23*).

The morphology and the local composition of the mixed oxides were examined by scanning electron spectroscopy (SEM) and semiquantitative X-ray fluorescence using a JEOL JM-35C electron microscope combined with an EDAX PV 9100 energy dispersive X-ray detector.

X-ray photoelectron (XPS) spectra were measured with an ESCA-750 Shimadzu spectrometer using Mg$K\alpha$ radiation. The Shimadzu spectrometer was operated at 8 kV and 30 mA and was interfaced to a computer for data collection and analysis. The binding energies were referenced to the C 1*s* peak from adventitious carbon at 285.0 eV. The quantitative composition was determined by considering a solid solution and using sensitivity factors measured in our spectrometer.

BET surface areas (Sg) were measured by N_2 adsorption at −195°C with a Micromeritics Accusorb 2100 sorptometer. The carbon content of the samples was measured by combustion volumetry. Chemical composition was determined by atomic absorption spectrometry (AAS).

Catalytic Tests

Catalytic tests were carried out in a fixed-bed, single-pass tubular reactor. The stainless-steel reactor was 50 cm long and 0.9 cm inside diameter. Reactor pressures were controlled with a Grove 91W back-pressure regulator. Samples were reduced *in situ* using a flowing 5 vol% H_2/Ar gas mixture at atmospheric pressure. Reduction was performed for 10 h at 275°C before synthesis gas exposure. A feed gas consisting of 60% H_2, 30% CO, and 10% N_2 was admitted to the reactor at a gas hourly space velocity of 5000 h^{-1}. All tests were performed at 50 atm and 275°C. Product analyses were made by gas chromatography using a Hewlett–Packard 5880 chromatograph. A thermal conductivity detector was employed to detect Ar, CO, and CO_2 after separation by a 3-m Porapak R column. Organic products were analyzed by flame ionization using a 50-m Hewlett–Packard HP-1 capillary column. Columns were located in a single oven, which was ramped from 10 to 225°C at 8°C min^{-1}. Product gas was sampled every 3 h. The CO–H_2 reaction was carried out for more than 30 h until steady-state conversion was obtained. Conversions were maintained at less than 10%.

RESULTS

1. Characterization of the Mixed Oxides

1a. Procedure I: Air 500°C–air 500°C. The X-ray diffractogram of the mixed oxide obtained from hydroxycitrate precursor A by using procedure I (Table 1) is shown in Fig. 1a. Two phases were detected: CuO and a spinel-like structure. The crystal sizes cal-

TABLE 1

Obtainment of Mixed Oxides: Consecutive Decomposition–Calcination Treatments of Hydroxycitrate Precursor A

Procedure	Decomposition[a] (atm, T_M)	Calcination[b] (atm, T_C)
I	Air, 500°C	Air, 500°C
II	N_2, 500°C	N_2, 500°C
III	N_2, 500°C	Air, 500°C
IV	N_2, 280°C	Air, 500°C

[a] Decomposition was performed from 25°C to T_M.
[b] Calcination was carried out at constant T_C for 8 h.

culated for both phases were similar (9.0 nm). Taking into account the metallic composition of the sample, a variety of copper, cobalt, and/or aluminum spinels, like Co_3O_4, $CoAl_2O_4$, $CuAl_2O_4$, $CuCo_2O_4$, or γ-Al_2O_3 could be formed. Many of these spinel phases display nearly coincident diffraction patterns (*24–26*). Consequently, the identity and chemical composition of the spinel phase detected in diffractogram 1a is difficult to specify from X-ray results alone.

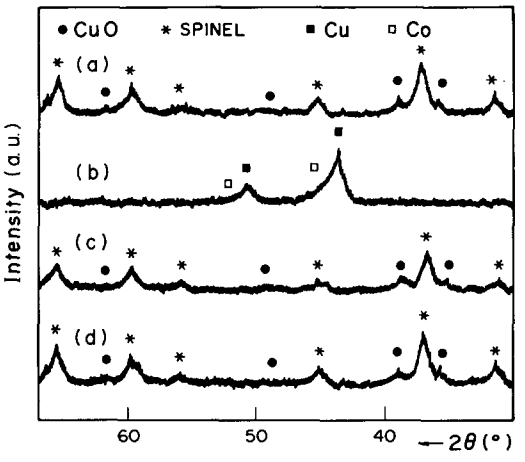

FIG. 1. Powder X-ray diffraction patterns of the mixed oxides obtained from hydroxycitrate precursor A by using different decomposition–calcination procedures. (a) Procedure I; (b) procedure II; (c) procedure III; (d) procedure IV. The characteristics of procedures I to IV are given in Table 1.

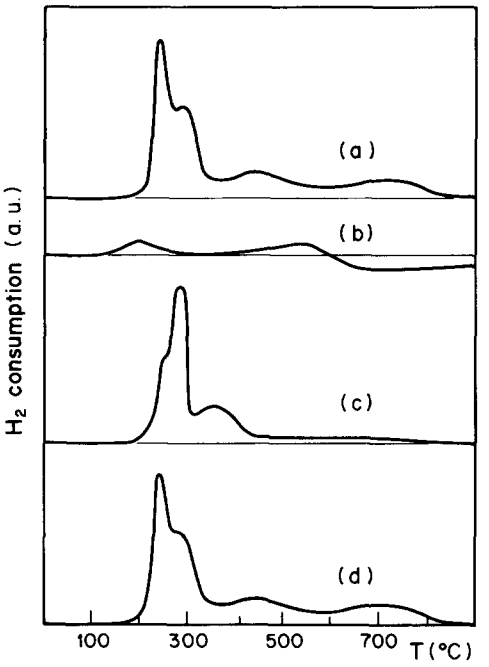

FIG. 2. TPR profiles of mixed oxides. Reductograms (a, b, c, and d): mixed oxides obtained through procedures I, II, III, and IV, respectively.

Temperature-programmed reduction was used as a complementary identification technique. The TPR profile shown in Fig. 2a exhibited a low-temperature peak at 250–280°C resulting from the reduction of Cu^{2+} (*7, 9, 27, 28*) and several reduction bands at higher temperatures that are attributed to the reduction of Co ions (*7, 9, 29*). The Cu^{2+} reduction peak presented a shoulder at about 300°C and the reduction of cobalt was achieved in two broad consumption bands. This suggested that both metals are present in several different phases having different reducibilities.

Surface characterization of Cu and Co species was performed by XPS. The respective spectra are shown in Figs. 3 and 4. The XPS spectra of CuO, Co_3O_4, and $CoAl_2O_4$ are included as reference. Cu^{1+} and Cu^0 can be distinguished from Cu^{2+} species by the Cu $2p_{3/2}$ binding energies and the lack of shake-up satellite peaks (*30–35*). In our case, the Cu $2p$ spectrum (Fig. 3, spectrum

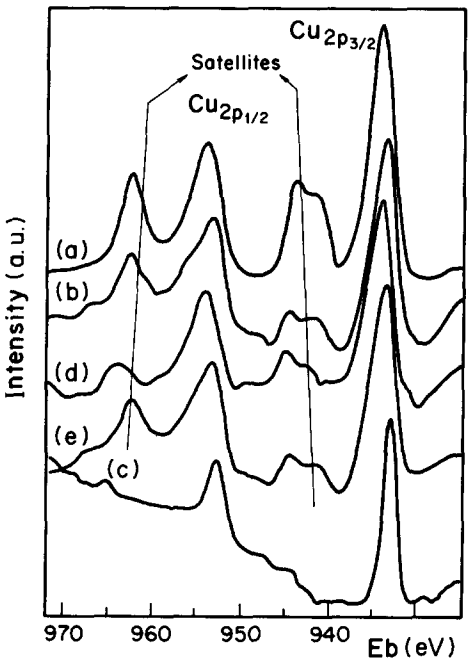

FIG. 3. Cu $2p$ XPS spectra of mixed oxides. Spectrum (a): CuO. Spectra (b, c, d, e): mixed oxides obtained through procedures I, II, III, and IV, respectively.

b) contained the intense satellite structure on the high-energy side, which is indicative of Cu^{2+} state and it was similar to the CuO spectrum (Fig. 3, spectrum a). In the case of Co, the Co $2p_{3/2}$ and Co $2p_{1/2}$ binding energies, as well as the shape of satellite peaks (Fig. 4, spectrum b), suggest the coexistence of Co^{2+} and Co^{3+} on the surface (*36–41*). In addition, the Co $2p$ spectrum closely resembled Co_3O_4 (Fig. 4, spectrum a). The quantitative analysis of the XPS peaks expressed by the Cu/Co atomic ratio is given in Table 2. A value of Cu/Co = 0.8 was obtained, which was slightly lower than the bulk composition ratio determined by AAS (Cu/Co = 0.96).

The SEM micrographs showed that the mixed oxide resembled that of a solid foam with an extremely open texture. This extensive porosity was produced by the evolution of gaseous decomposition products. The BET surface area was 63 $m^2\ g^{-1}$ (Table 2) and the amount of carbon was lower than 0.5%.

1b. Procedure II: N_2 500°C–N_2 500°C. The XRD characterization of the mixed oxide obtained through procedure II showed the presence of metallic Cu and Co phases (Fig. 1b), thereby indicating that inert gas decomposition–calcination causes the reduction of the Cu and Co ions originally present in the hydroxycitrate precursor. The X-ray diffraction pattern corresponding to Cu^0 appeared clearly defined once procedure II was completed, but in the case of Co an additional N_2 treatment at 600°C was necessary to detect the Co^0 phase. The Cu^0 crystallite size determined by X-ray diffraction line broadening of the Cu^0 (111) line was

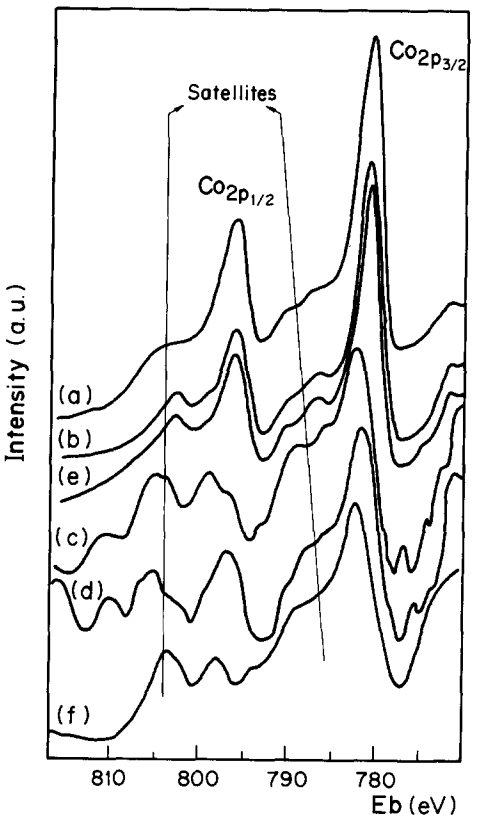

FIG. 4. Co $2p$ XPS spectra of mixed oxides. Spectra (a, f): Co_3O_4 and $CoAl_2O_4$, respectively. Spectra (b, c, d, e): mixed oxides obtained through procedures I, II, III, and IV, respectively.

TABLE 2

Effect of the Decomposition–Calcination Procedure: XPS and BET Results

Procedure[a]	XPS Binding energies		Atomic ratios		Sg[b] (m^2/g)
	Cu $2p_{3/2}$ (eV)	Co $2p_{3/2}$ (eV)	Cu/Co	C/Cu	
I	933.5 (3.2)[c]	780.7 (3.4)	0.8	43	63
II	932.8 (1.8)	782.5 (7.5)	1.2	250	8
III	934.0 (3.4)	781.3 (6.7)	4.1	60	14
IV	933.4 (3.3)	780.5 (3.2)	0.9	51	62
CuO	933.3 (3.2)				
$CuAl_2O_4$	934.2 (3.3)				
Co_3O_4		780.5 (3.5)			
$CoAl_2O_4$		782.6 (6.5)			

[a] As in Table 1.
[b] BET surface areas.
[c] Values in parentheses are full width at half maximum (FWHM).

14.0 nm (major Cu^0 diffraction line at ca. 43.3° in 2θ).

The TPR profile (Fig. 2, curve b) exhibited two small consumption bands with maxima at 200 and 550°C, respectively. The low TPR H_2 uptakes confirmed that most Cu and Co ions were reduced during decomposition–calcination of the precursor under N_2. The two small consumption bands detected in the reductogram can be attributed to the surface reoxidation of the metallic crystallites upon exposure to air at room temperature. For temperatures higher than 600°C, a negative consumption band was detected. The appearance of such a negative band is attributed to the formation of CH_4 at high temperatures by hydrogenation of remaining carbon on the decomposed sample. The quantity of residual carbon determined by combustion volumetry was significant (8 wt%).

Figure 3, spectrum c, shows the Cu $2p$ XPS spectrum. The Cu $2p_{3/2}$ lines did not exhibit the high-energy satellite peaks that are indicative of the presence of Cu^{2+} species. The values of binding energy (BE) and full width at half maximum (FWHM) of the Cu $2p_{3/2}$ peak are given in Table 2. The peak became narrower (FWHM = 1.8 eV) and had BE values corresponding to either Cu_2O or Cu^0 (*33*, *42*). The weak signal obtained for Co $2p$ spectrum (Fig. 4, spectrum c) did not allow a good identification. Nevertheless, the BE and FWHM values (Table 2) as well as the satellite structure resembled $CoAl_2O_4$ (Fig. 4, spectrum f). Surface composition derived from XPS intensities is reported in Table 2. The Cu/Co ratio was similar to that obtained from bulk composition. The C/Cu surface ratio was approximately sixfold the value determined for the mixed oxide obtained through procedure I, which agrees with the significant amount of residual carbon detected by combustion volumetry on the sample decomposed according to procedure II.

The mixed oxide obtained by using procedure II was also characterized by scanning electron microscopy. When compared with SEM micrographs of the mixed oxide obtained through procedure I, it was observed that although the morphology was similar, the porosity of the agglomerates diminished. The BET surface area was low (ca. 10 m^2 g^{-1}, Table 2).

1c. Procedure III: N_2 500°C–Air 500°C.

Precursor A was decomposed in N_2 up to 500°C and then calcined in air at 500°C for 8 h (Table 1, procedure III). The X-ray diffractogram of the resulting mixed oxide (Fig. 1c) revealed the presence of CuO and a spinel structure, which are the principal crystalline phases detected in the mixed oxide obtained by using procedure I (Fig. 1a). Nevertheless, the TPR characterization showed different reductograms (Fig. 2, curves a and c). Although in reductogram 2c the reduction of copper is achieved in two superimposed peaks at approximately 240 and 300°C similarly to reductogram 2a, the relative importance of these two peaks is clearly different. In contrast to reductogram 2a, in reductogram 2c the reduction peak with maximum at 300°C was bigger than the peak at 240°C. On the other hand, the reduction of cobalt ions exhibited two consumption bands: a broadband at middle temperature (320–480°C) and an almost continuous band from 480°C to approximately 800°C.

The XPS results are given in Table 2 and Figs. 3 and 4. The shape and the satellite structure of the Cu 2*p* spectrum (Fig. 3, spectrum d), as well as the BE and FWHM values (Table 2), revealed the presence of Cu^{2+} species. It is clear that calcination in air at 500°C eliminates the residual carbon and oxidizes the metallic Cu crystallites formed during the initial N_2 decomposition up to 500°C. The Cu $2p_{3/2}$ binding energies could be used to distinguish between $CuAl_2O_4$ and CuO on the surface of the samples (Table 2). However, the Cu $2p_{3/2}$ line for the mixed oxides obtained through procedure III laid between the values obtained for CuO and $CuAl_2O_4$. Indeed, the reproducibility of the measurements of the sample varied as much as ±0.3 eV. Such a variation in the Cu $2p_{3/2}$ peak position is characteristic of a surface having mixed species (*33, 35*).

The Co 2*p* XPS spectrum is shown in Fig. 4, spectrum d. Although the XPS signal was weak, the binding energy, line shape, and satellite intensity suggested the presence of a surface Co^{2+} phase. Additionally, the spectrum was consistent with $CoAl_2O_4$ taken as reference (Fig. 4, spectrum f).

The Cu/Co atomic ratio measured by XPS on the sample surface was 4.1, which is four times higher than the value expected (0.96) on the basis of chemical analysis. This strongly indicates that a Cu-rich layer formed on the sample surface. The surface C/Cu molar ratio (Table 2) was similar to that determined in the case of procedure I.

The BET surface area was 14 $m^2\ g^{-1}$ thereby indicating that the carbon burning by air at 500°C produced only a slight surface area increase.

1d. Procedure IV: N_2 280°C–air 500°C. The XRD and TPR characterizations of the mixed oxide obtained using procedure IV (N_2 280°C–air 500°C) indicate that the number and kind of phases present in the solid, as well as their relative composition, were similar to those detected in the mixed oxide obtained through procedure I (air 500°C–air 500°C). In fact, the XRD pattern (Fig. 1d) revealed the presence of CuO and a spinel phase and was very similar to diffractogram 1a. The TPR trace (Fig. 2, curve d) was essentially identical with reductogram 2a, showing the low-temperature reduction band attributed to the reduction of copper and the two high-temperature bands caused by the reduction of the Co ions.

The XPS Cu 2*p* and Co 2*p* spectra are given in Figs. 3 and 4, respectively. The shape and the satellite structure of the Cu 2*p* spectrum (Fig. 3, spectrum e) indicated the presence of surface Cu^{2+} ions. The BE of the Cu $2p_{3/2}$ peak was close to the corresponding BE value obtained for CuO (Table 2). The Co 2*p* spectrum (Fig. 4, spectrum e) resembled Co_3O_4 (Fig. 4, spectrum a), revealing the coexistence of Co^{2+} and Co^{3+} on the surface.

The surface Cu/Co molar ratio (Table 2) was similar to that determined for the entire volume, thereby suggesting a uniform distribution of the metal ions. XPS results (Table 2) and combustion-volumetry analysis ($C <$ 0.5 wt%) showed that the level of residual carbon was not significant.

Finally, the textural characterization gave

TABLE 3

Effect of the Decomposition–Calcination Procedure: Catalyst Testing

Conditions: steady state; P = 50 atm; T = 275°C, GHSV = 5000 h^{-1}; H_2/CO = 2

Procedure[a]	Activity (μmol CO/g cat/min)	Selectivity[b] (wt%) · product distribution (α)[c]					
		HC[d]	Alc[d]	CH_3OH	C_2^+OH[d]	CH_4	C_2^+H[d]
I	93.2	48.3 (α = 0.44)	51.7 (α = 0.36)	28.4	23.3	19.2	29.1
II	2.1	70.3	29.7	25.4	4.3	40.1	30.2
III	15.2	45.8 (α = 0.39)	54.2	49.2	5.0	25.3	20.5
IV	98.0	46.0 (α = 0.46)	54.0 (α = 0.38)	29.2	24.8	16.4	29.6

[a] As in Table 1.

[b] Excluding water and carbon dioxide.

[c] Absence of an α value indicates that the C_1 product falls out of the Schulz–Flory plot.

[d] HC, hydrocarbons; Alc, alcohols; C_2^+OH, all alcohols except methanol; C_2^+H, all hydrocarbons except methane.

a surface area of 62 m^2 g^{-1}, which was approximately the same as that determined for the mixed oxide obtained through procedure I (Table 2).

2. *Catalytic Measurements*

The catalytic results are presented in Table 3. In all cases only hydrocarbons and linear alcohols were obtained. No aldehydes or other oxygen-containing products were observed. The selectivity toward alcohols gradually increased until steady state was reached after approximately 30 h. Excessive methane formation during the start-up was not noted.

Catalysts obtained from precursor A by using, respectively, procedures I and IV exhibited similar catalytic behavior producing 46–48 wt% of hydrocarbons, 52–54 wt% of total alcohols, and 23–25 wt% of higher alcohols. The observed catalytic activities are comparable to those determined by other authors under similar operational conditions (*12, 21, 43*). Product distributions were consistent with the Schulz–Flory equation and chain growth probability factors (α) were determined. The chain propagation factor for alcohol products was α = 0.36–0.38, including the formation of methanol up to *n*-hexanol. In the case of hydrocarbons, the formation of linear paraffins and linear olefins fell on the same straight line of the Schulz–Flory plot. Values of α = 0.44–0.46 were obtained, which differ from those of the alcohol products and indicate that higher-molecular-weight products were formed. This was verified by experimental data since linear hydrocarbons up to C_9 were detected.

The catalyst obtained by using procedure II presented very low activity. The fraction of ethanol and higher alcohols in the products decreased to 4.3% and, as a consequence, the overall alcohol selectivity was only 29.7 wt%. Hydrocarbons were the dominant products and a dramatic increase in the methane formation was observed (40.1 wt%).

The catalytic activity of the mixed oxide obtained from decomposition of precursor A using procedure III was 15.2 μmol CO converted/g cat/min. On a surface area basis this value is 1.09 μmol CO/m^2 cat/min, which is comparable with the catalytic activities of the samples obtained by using either

procedure I (activity = 1.48 μmol CO/m^2 cat/min) or procedure IV (activity = 1.58 μmol CO/m^2 cat/min). Nevertheless, the relative product composition was different since the selectivities to C_1 products, especially to methanol, were clearly enhanced. The selectivity to methanol was 50.2 wt%, which represents nearly 90% of the alcohol production. The fraction of methane was 25.3 wt% and the average molecular weight of hydrocarbon products slightly decreased (α = 0.39).

DISCUSSION

Mixed Oxides from Procedures I and IV

Since the two mixed oxides obtained from precursor A by using, respectively, procedures I and IV exhibited similar physicochemical and catalytic properties, the discussion below refers to both samples.

The mixed oxides presented two crystalline phases (CuO and a spinel structure) with small crystallite sizes. Regarding the spinel phase, it has been stated that the oxygen calcination up to 650°C causes the partial oxidation of Co^{2+} to Co^{3+} (*29*). Thus, the formation of spinel-type phases like Co_3O_4, $CoAl_2O_4$, and $CuCo_2O_4$ can be expected. The diffraction patterns of these spinel compounds closely coincide (*26*). On the other hand, $CuAl_2O_4$ and γ-Al_2O_3 are also spinel structures with almost identical diffraction peaks (*35*). The chemical composition of the spinel structure found in this study was therefore difficult to establish using only XRD characterization.

Temperature-programmed reduction proved to be a useful identification technique since it is well known that the number of Al^{3+} ions in the vicinity of Co (or Cu) ions determines the TPR reduction temperature (*29, 44*). The TPR trace showed that the reduction of copper was achieved in two overlapping peaks with maxima at 240 and 300°C, respectively. The peak at 240°C is attributable to the reduction of CuO (*9*). The high-temperature peak at 300°C appeared as a shoulder and revealed the presence of an additional amorphous phase, probably a surface $CuAl_2O_4$ spinel formed by dispersion of copper ions on the surface defect spinel of the alumina support (*27*). Although a bulk $CuAl_2O_4$ phase is thermodynamically unstable at temperatures below 600°C (*45, 46*), the formation of a "copper surface spinel," where the Cu^{2+} ions are in a distorted octahedral geometry, has been reported at temperatures as low as 300°C (*47*). Clausen *et al.* (*48*) have already noted by using *in situ* X-ray absorption spectroscopy (XAS) that in Cu–Zn–Al catalysts the strong interaction between the copper and aluminum species diminishes the reducibility of Cu^{2+} ions. Similar results were obtained by Gusi *et al.* (*44*).

The reduction of Co species presented two broad consumption bands at 340–560°C and 560–850°C, respectively. Monometallic Co_3O_4 oxide reduces in the region corresponding to the low-temperature band (*7, 41*). Although the reduction of Co^{3+} ions in bulk Co_3O_4 can occur through a consecutive reduction mechanism like $Co^{3+} \rightarrow Co^{2+} \rightarrow Co^0$ (*7, 23*), the reduction of Co^{3+} and Co^{2+} to metal during TPR of the mixed oxides generally is achieved in only one peak (*29*). On the other hand, the reducibility of Co^{2+} ions in a $CoAl_2O_4$ spinel phase decreases because the Al^{3+} ions in the surrounding of the Co^{2+} ions polarize the covalent Co–O bonds and thereby increase the effective charge of the Co ions (*29, 49*). As a consequence, the lattice energy increases and the Co^{2+} reduction peak is shifted to higher temperatures. However, formation of a $CoAl_2O_4$ spinel phase at mild temperatures normally leads to a partly inverse spinel, which is unstable with respect to the normal $CoAl_2O_4$ spinel. The Co^{2+} ions occupy the tetrahedral sites (Co_{td} ions) in a normal spinel because of the favorable relative octahedral site preference energy of Al^{3+} ions with respect to Co^{2+} ions (*45*). The stability of Co^{2+} in a tetrahedral configuration explains the well-known resistance to reduction of Co_{td} ions (*50, 51*). In a partly inverse spinel, some of the Co^{2+} ions are located in octahedral sites (Co_{oh} ions) and are readily reduced

in the 340–560°C low-temperature region (*39*). The reduction of both, Co_{td} and Co_{oh} ions, is catalyzed by the presence of metallic copper (*7*). Thus, the reduction of Co in the mixed oxide can be explained by considering that the low-temperature reduction band at 340–560°C is caused by the reduction of Co_3O_4 and Co_{oh} ions in a partly inverse $CoAl_2O_4$ spinel phase and that the high-temperature reduction band represents the reduction of Co_{td} ions in the normal $CoAl_2O_4$ spinel.

In conclusion, the decomposition–calcination of precursor A by either procedure I or IV caused the formation of monometallic CuO and Co_3O_4 oxides, and binary oxides with high M^{2+}–M^{3+} interaction. The $CoAl_2O_4$ and $CuAl_2O_4$ aluminates can be chemically represented as $MO \cdot Al_2O_3$, i.e., metal oxides filling specific lattice sites of Al_2O_3. The XPS characterization showed that the surface species were mostly CuO and Co_3O_4 and that the distribution of the metals in the solid was uniform.

According to our TPR data, the reduction with H_2 at 275°C for 10 h performed *in situ* before the catalytic runs would reduce Cu^{2+} species to Cu^0 and surface Co_3O_4 to Co^{2+} and probably to metallic Co. Because of the low reducibility of Co^{2+} ions located in the alumina matrix, the $CoAl_2O_4$ phase would not be affected by such a hydrogen treatment. To verify this assumption we performed some additional XRD characterization of the samples after reduction. The X-ray diffractograms of the H_2-exposed catalysts showed that the spinel phase was only slightly modified by the hydrogen treatment. No additional phases were detected. Thus, in a simple representation, the catalysts after reduction would be composed of metallic Cu–Co particles homogeneously supported on a $CoAl_2O_4$ spinel-like phase.

The catalysts presented catalytic activity values similar to those determined by other researchers who have used Cu/Co/Al(Cr) catalysts prepared by either coprecipitation or complexation methods (*12, 21, 43*). The alcohol fraction in the products was 52–54 wt% and the selectivity to ethanol and higher alcohols (23–25 wt%) was rather high taking into account that no alkali was added to the samples. Promoting Cu–Co catalysts with alkali increases oxygenate selectivity at the expense of hydrocarbons (*6, 52*). The exact nature of the active sites responsible for the formation of higher alcohols on supported Cu–Co catalysts is still a subject of debate. While some authors have suggested that optimum catalysts result from a synergism between small Cu–Co bimetallic clusters (*6*), there are also a number of reports that postulate that the formation of ethanol and higher alcohols is due to the combination of Co ions in a spinel-like phase with either a Cu (*25*) or a Cu–Co metallic phase (*53*). Our data do not allow us to distinguish between these two postulates. Nevertheless, it must be noted here that after reduction the catalysts obtained by using procedures I and IV contained the two kinds of active centers (metallic Cu–Co particles and Co^{2+} in a spinel-like structure), which acting separately or in combination would be responsible for the formation of higher alcohols.

Mixed Oxides from Procedures II and III

The mixed oxides obtained from decomposition–calcination of precursor A by using procedure II were markedly different from those obtained through procedures I and IV. In fact, the X-ray diffractograms showed the presence of Cu and Co in metallic states; no metal oxide phase was detected. This indicates that at least one of the gaseous products generated during the decomposition under nitrogen acts as a reducing agent of the copper and cobalt oxides species originally present in the precursors. In a recent paper (*54*), we reported the results of studies of the decomposition mechanism of the Cu–Co–Al mixed hydroxycitrates under air and nitrogen atmospheres by employing the evolved gas analysis (EGA) technique. We found that during the temperature-programmed decomposition of these metal hydroxycitrates under nitrogen,

CO is generated at approximately 220°C and its concentration increases rapidly with a maximum at ca. 300°C. We concluded that the metal oxides (CuO, CoO), which are probably formed from the beginning of the high-temperature decomposition step, are reduced in the presence of CO in the gaseous products.

The TPR traces showed two small consumption bands, at 220 and 500°C, respectively. The low-temperature peak, which is attributable to the reduction of Cu^{2+} species, appeared shifted to lower temperatures considering that the bulk CuO phase reduces at ca. 240°C. The characteristics of this reduction peak (low H_2 consumption, maximum shifted to lower temperatures) are consistent with formation of a surface oxide layer on the metallic Cu crystallites. The peak at 500°C corresponded to reduction of cobalt oxide species, presumably Co^{2+} considering that the decomposition was performed under nitrogen. Since reduction of Co^{2+} ions to metallic Co is achieved at much lower temperature in the CoO phase (approximately 400°C, Ref. (*9*)), this high-temperature band was probably caused by the reduction of the Co^{2+} ions in a spinel phase of $CoAl_2O_4$. The amounts of Cu and Co calculated from the TPR peak areas were 3.4 and 5.7%, respectively. These values were clearly lower than the actual composition of the samples (22.4% Cu and 22.7% Co), thereby confirming that only a small fraction of the metals remained in an oxidic phase after the decomposition in N_2.

High concentration of residual carbon interfered with XPS characterization of the samples. In spite of the weak intensity signals, the analysis of the XPS spectra revealed the presence of Cu^0 and Co^{2+} species, the latter presumably as $CoAl_2O_4$. This surface characterization confirmed that reoxidation, if any, of the large Cu^0 crystallites was limited to the external monolayers. On the contrary, only Co^{2+} species were detected on the surface of the samples, which is not surprising since it is well known that Co^0 is readily reoxidized upon exposure to air at room temperature (*38, 55*). The presence of a bulk Co^0 phase as identified by X-ray diffraction can be explained by considering that the surface residual carbon acts as a protective layer, which makes the diffusion of the oxygen molecules difficult.

These catalysts exhibited low activity, probably because of the partial blockage of the active sites by the high level of residual carbon, as was suggested by the XPS characterization. On the other hand, the selectivity to hydrocarbons was enhanced up to 70 wt%, increasing especially the CH_4 concentration (40 wt%). The high methanation activity may be readily explained by the presence of a large amount of metallic cobalt resulting when decomposition–calcination procedure II was used. The presence of large metallic Cu crystallites may also be a contributing factor in enhancing hydrocarbon selectivity since it has been reported that oxygenate synthesis decreases when the Cu metal dispersion is decreased (*25*). Although the selectivity to methanol was still significant (25 wt%), the formation of ethanol and higher alcohols was almost completely suppressed. The loss of the active sites for higher alcohols synthesis must be related to the poor interaction between copper and cobalt. In fact, the presence of both, small metallic Cu–Co clusters and Cu/Co^{2+} spinel centers that favor component synergism were not observed in samples obtained by using procedure II.

Through procedure III, precursor A was decomposed in N_2 up to 500°C and then calcined in air at the same temperature for 8 h. This procedure regenerated the metal oxide phases and eliminated almost completely the residual carbon. Qualitatively, the amorphous and crystalline phases detected by TPR and XRD techniques were the same as those observed in the mixed oxides obtained by using procedures I and IV, i.e., CuO, Co_3O_4, $CoAl_2O_4$, and $CuAl_2O_4$. However, the relative concentration of these oxidic phases was different. In fact, the amounts of $CuAl_2O_4$ and $CoAl_2O_4$ were significantly

higher in the mixed oxides obtained through procedure III. This can be explained on the basis of the protective effect played by the residual carbon remaining on the sample surface after the initial decomposition in N_2 up to 500°C. Since this residual carbon burns at ca. 350°C when exposed to air at increasing temperatures (*16*), it is conceivable that a major part of the bulk Cu^0 and Co^0 phases formed upon N_2 decomposition was preserved from air reoxidation until the carbon burning takes place during the air calcination step. This interpretation implies that the metal oxide phases are formed through a mechanism different than that obtained using procedure I. Besides, AAS and XPS data showed that the distribution of the metals in the entire solid was inhomogeneous. A Cu-rich layer was formed at the catalyst surface at expense of surface Co concentration, as a Cu/Co ratio of 4.1 was detected.

The catalyst obtained by using procedure III exhibited activity per surface area unit similar to those of catalysts obtained from procedures I and IV. However, the selectivity shifted toward greater methanol formation. The methanol synthesis was increased up to 50.2 wt%, whereas formation of ethanol and higher alcohols was only 5.0 wt%. The higher selectivity to methanol is consistent with the presence of a surface Cu-rich layer in the catalyst. At the same time, the significant amount of surface enrichment by copper at the expense of surface cobalt concentration decreased the selectivity to higher alcohols. This result is in line with previous work (*7, 13*), which emphasized the importance of obtaining a homogeneous distribution of the metals to enhance higher alcohols synthesis. The selectivity to hydrocarbons was 45.8 wt% increasing the CH_4 fraction to 25.3 wt%. The chain growth probability factor for hydrocarbons was not changed significantly (α = 0.39). This is lower than a cobalt Fischer–Tropsch distribution, but it is similar to the values reported for Cu–Co based catalysts (*21, 43*).

CONCLUSIONS

The effect of the decomposition–calcination procedure of Cu/Co/Al citrate precursors on the physicochemical properties of the resulting mixed oxides and on the catalytic activity and selectivity for synthesis gas conversion to methanol and higher alcohols can be summarized as follows:

1. The decomposition–calcination in nitrogen (procedure II) yielded solids containing Al_2O_3, bulk Cu^0 and Co^0 phases, and surface CuO, Cu^0, and $CoAl_2O_4$ phases. The solids exhibited low specific surface areas, sintered metallic crystallites, a high level of residual carbon, and a poor interaction between the metal elements. As a consequence, the catalytic activity was low and the formation of ethanol and higher alcohols was suppressed.

2. The N_2 500°C–air 500°C treatment (procedure III) regenerated the metal oxide phases and eliminated any trace of residual carbon. However, the mixed oxides had low specific surface areas and presented an inhomogeneous distribution of the metal ions. Because of this latter factor, these catalysts had poor selectivity to higher alcohols.

3. The mixed oxides obtained by using procedures I (decomposition–calcination in air) and IV (N_2 280°C–air 500°C), presented similar physicochemical properties and catalytic activities. The solids contained surface CuO and Co_3O_4 oxides likely supported on a $Co(Cu)Al_2O_4$ spinel phase. The distribution of the metals was uniform and the surface area values were high. These catalysts exhibited higher catalytic activities and were selective for the formation of alcohols, producing 52–54 wt% of total alcohols and 23–25 wt% of ethanol and higher alcohols. However, while procedure IV prevented a rapid and energetic decomposition of hydroxycitrate precursors, procedure I involved a highly exothermic decomposition, which was extremely difficult to control. Thus, procedure IV was found to be the most appropriate of the decompo-

sition–calcination treatments studied in the present work.

4. The catalytic results showed that catalyst preparation is a critical factor affecting both activity and selectivity. A homogeneous distribution of the metal elements (Cu and Co) seems to be a prerequisite for higher alcohols synthesis. In agreement with previous work, we found that cobalt ions in combination with metallic Cu or Cu–Co phases are important for oxygenate synthesis.

ACKNOWLEDGMENTS

Support of this work by the Consejo Nacional de Investigaciones Cientificas y Técnicas (CONICET, Argentina) and Yacimientos Petroliferos Fiscales (YPF) is gratefully acknowledged.

REFERENCES

1. Sugier, A., and Freund, E., US Patent 4,112,110, Institut Français du Pétrole, 1978.
2. Sugier, A., and Freund, E., GB Patent 2,037,179, Institut Français du Pétrole, 1979.
3. Hardman, H., and Beach, R., US Patent Appl. 905,703, Standard Oil Co., 1978.
4. Greene, M., and Gelbein, A., US Patent 4,477,594, Chem. Systems, Inc., 1984.
5. Arlie, J. P., Cariou, J. P., Courty, P., and Travers, P., *in* "Proceedings, 6th International Symp. on Alcohol Fuel Technology," Vol. II, pp. 92–99. Ottawa, 1984.
6. Courty, P., Durand, D., Freund, E., and Sugier, A., *J. Mol. Catal.* **17,** 241 (1982).
7. Grandvallet, P., Courty, P., and Freund, E., *in* "Proceedings, 8th International Congress on Catalysis, Berlin, 1984," Vol. II, pp. 81–92. Dechema, Frankfurt-am-Main, 1984.
8. Marchi, A. J., Di Cosimo, J. I., and Apesteguia, C. R., *in* "Proceedings, 4th International Symp. on Scientific Bases for the Preparation of Heterogeneous Catalysts," Louvain-la Neuve, paper H-7, 1986.
9. Marchi, A. J., Di Cosimo, J. I., and Apesteguia, C. R., *in* "Proceedings, 9th International Congress on Catalysis" (J. M. Phillips and M. Ternan, Eds.), Vol. 2, pp. 529–536. Chem. Institute of Canada, Ottawa, 1988.
10. Errani, E., Fornasari, G., La Torretta, T., Trifiro, F., and Vaccari, A., *in* "Proceedings, 11th Iberoamerican Symposium on Catalysis," Vol. 3, pp. 1239–1247. Instituto Mexicano del Petroleo, Mexico, 1988.
11. Cao, R., Pan, W. X., and Griffin, G. I., *Langmuir* **4,** 1108 (1988).
12. Baker, J. E., Burch, R., and Golunski, S. E., *Appl. Catal.* **53,** 279 (1989).
13. Xiaoding, X., Doesburg, E., and Scholten, J., *Catal. Today* **2,** 125 (1987).
14. Mazanec, T. J., *J. Catal.* **98,** 115 (1986).
15. Smith, K., and Anderson, R., *J. Catal.* **85,** 428 (1984).
16. Di Cosimo, J. I., and Apesteguia, C. R., *J. Catal.* **116,** 71 (1989).
17. Paris, J., and Paris, R., *Bull. Soc. Chim. Fr.* **4,** 1138 (1965).
18. Rousset, A., and Paris, J., *Bull. Soc. Chim. Fr.,* 446 (1969).
19. Marcilly, C., Courty, P., and Delmon, B., *J. Am. Ceram. Soc.* **53,** 56 (1970).
20. Shanon, I. R., *Chem. Ing.,* 149 (1971).
21. Sheffer, G. R., and King, T. S., *Appl. Catal.* **44,** 153 (1988).
22. Zhang, H. M., Teraoka, Y., and Yamazoe, N., *Chem. Lett.* **4,** 665 (1987).
23. Marchi, A. J., Ph.D. thesis, Universidad Nacional del Litoral, Santa Fe, Argentina, 1988.
24. Greenwood, N. N., "Ionic Crystals, Lattice Deffects and Nonstoichiometry." Butterworths, London, 1968.
25. Sheffer, G. R., Jacobson, R. A., and King, T. S., *J. Catal.* **116,** 95 (1989).
26. Inorganic Index to the Powder Diffraction File, pp. IV–X, Joint Committee on Powder Diffraction Standards, USA, 1974.
27. Lo Jacono, M., Cimino, A., and Inversi, M., *J. Catal.* **76,** 320 (1982).
28. Dumas, J., Geron, C., Kribi, A., and Barbier, J., *Appl. Catal.* **47,** 19 (1989).
29. Arnoldy, P., and Moulijn, J. A., *J. Catal.* **93,** 38 (1985).
30. Wohlberg, A., Ogilvie, J., and Roth, J. F., *J. Catal.* **19,** 86 (1970).
31. McIntyre, N. S., and Cook, M. G., *Anal. Chem.* **47,** 13, 2208 (1975).
32. Shreifels, J., Rodero, A., and Swartz, W., *Appl. Spectrosc.* **33**(4), 380 (1979).
33. Strohmeier, B. R., Leyden, D. E., Field, R. S., and Hercules, D. M., *J. Catal.* **94,** 514 (1985).
34. Di Castro V., Furlani, C., Gargano, M., and Rossi, M., *Appl. Surf. Sci.* **28,** 270 (1987).
35. Friedman, R., Freeman, J., and Lytle, F., *J. Catal.* **55,** 10 (1978).
36. Okamoto, Y., Nakano, H., Imanaka, T., and Tekanishi, S., *Bull. Chem. Soc. Jpn.* **48,** (4), 1163 (1975).
37. Oku, M., and Hirokawa, K., *J. Electron Spectrosc. Relat. Phenom.* **8,** 475 (1976).
38. Moyes, R. B., and Roberts, M. W., *J. Catal.* **49,** 216 (1977).
39. Chin, R. L., and Hercules, D. M., *J. Phys. Chem.* **86,** 360 (1982).
40. Stranick, M., and Houalla, M., and Hercules, D., *J. Catal.* **104,** 396 (1987).
41. Castner, D. G., and Santilli, D. S., *in* "Catalytic

Materials: Relationship between Structure and Reactivity," ACS Symposium Series, Vol. 248, pp. 39–56. American Chemical Society, Washington, DC, 1984.

42. Liu, D., Zhu, Q., and Li, I., *in* "Proceedings, 9th International Congress on Catalysis" (M. J. Phillips and M. Ternan, Eds.), pp. 577–584. Chem. Institute of Canada, Ottawa, 1988.
43. Pan, W. X., Cao, R., and Griffin, G. L., *J. Catal.* **114,** 447 (1988).
44. Gusi, S., Triffiro, F., and Vaccari, A., *React. Solids* **2,** 59 (1986).
45. Navrotsky, A., and Kleppa, O. J., *J. Inorg. Nucl. Chem.* **29,** 2701 (1967).
46. Marques, E., Friedman, R., and Dahm, D., *Appl. Catal.* **19,** 387 (1985).
47. Wolberg, A., and Roth, J. F., *J. Catal.* **15,** 250 (1969).
48. Clausen, B., Lengler, B., Rasmussen, B., Niemann, W., and Topsoe H., *J. Physc.* **47**(8), 237 (1982).
49. Kung, H. H., *J. Catal.* **73,** 387 (1982).
50. De Clerk-Grimee, R., Canesson, P., Friedman, R., and Fripiat, J., *J. Phys. Chem.* **82,** 885 (1978).
51. Chung, K. S., and Massoth, F. E., *J. Catal.* **64,** 320 (1980).
52. Calverly, E. M., and Anderson, R. B., *J. Catal.* **104,** 434 (1987).
53. Baker, J. E., Burch, R., and Yuqin, N., *J. Catal.* **73,** 135 (1991).
54. Di Cosimo, J. I., Marchi, A. J., and Apesteguia, C. R., *Thermochim. Acta*, in press.
55. Wang, N., Kaiser, U., Gauschow, O., Wiedmann L., and Benninghooven, A., *Surf. Sci.* **124,** 51 (1983).